*Desalination and Water Treatment*
www.deswater.com

doi: 10.5004/dwt.2022.28281

252 (2022) 66–76
March

# A hybrid polysulfone/mesoporous silica ultrafiltration membranes for industrial wastewater treatment

Ahmed Alharbi[a], Ahmed M. Desouky[b], Seif Bayoumi[c], Ahmed Shahat[d,*], Mohamed E.A. Ali[b,*]

[a]*Department of Chemistry, Faculty of Applied Science, Umm Al-Qura University, 21955 Makkah, Saudi Arabia*
[b]*Egypt Desalination Research Center of Excellence (EDRC) & Hydrogeochemistry Department, Desert Research Center, Cairo 11753, Egypt, email: m7983ali@gmail.com (M.E.A. Ali)*
[c]*Mechanical Engineering Department, Arab Academy for Science Technology and Maritime Transport, P.O. Box: 1029, Alexandria, Egypt*
[d]*Department of Chemistry, Faculty of Science, Suez University, Suez, Egypt, email: ashahat@aucegypt.edu (A. Shahat)*

Received 1 September 2021; Accepted 6 February 2022

**ABSTRACT**

Water permeability and dye rejection were considerably enhanced when mesoporous silica nanosphere (MSN) was added to the membrane matrix. The dry/wet phase conversion approach was used to create all membranes. The effect of MSN concentration (0%–8% wt.%) on the behavior of the PSF-UF membrane in the presence of polyvinylpyrrolidone (PVP) as a producing-pore agent was examined. When the MSN level was increased to 6 wt.%, the rejection of Crystal violet dye rose continuously. Scanning electron microscopy was utilized to analyze the morphological characteristics of ultrafiltration (UF) membranes. Polysulfone (PS)/PVP/$SiO_2$ (6%), for example, experienced high dye rejection (88.3%). The membrane permeability dropped from 415.9 L/$m^2$ h for PS/PVP to 122.7 L/$m^2$ h for PS/PVP/$SiO_2$ (6%) membrane when the MSN concentration increased to 6 wt.%. Only water could flow through the hydrophilic membrane on the feed side, resulting in a high-quality stream of water on the permeate portion, making the membrane suitable for the treatment of industrial effluent. The membrane's performance was improved by the addition of polyvinylpyrrolidone.

*Keywords:* Ultrafiltration; Crystal violet; Mesoporous silica nanosphere; Wastewater treatment

## 1. Introduction

Water's importance in human life cannot be overstated, since it is necessary for a broad range of activities, including home usage, recreation, power generation, agriculture, and industry, to name a few. Considering the rising need for drinking water in recent years, more current studies on water treatment have been produced [1]. In the textile and dyeing sectors, dyes are widely used, and their use is growing. Synthetic dyes are produced by over 0.7 million tons per year all over the world. In addition to squandering a substantial quantity of chemicals and water, releasing badly treated textile waste into the environment has the potential to cause several health and environmental issues. When exposed to normal treatment techniques, most dyes are poisonous and organically carcinogenic because of their complex aromatic ring structure. They're also resistant to disintegration or degeneration on a physiological level. It is therefore critical to create a method that can effectively remove these colors from effluents. There are several chemical, physical, and biological methods for removing colors from effluents available today. Each one has its own set of benefits and drawbacks [2–4]. All traditional and

* Corresponding authors.

contemporary wastewater treatment systems use membrane separation techniques, which are the most cost-effective, highly selective, and easy to combine with other processes. Membrane separation techniques are also the least harmful to the environment [5]. All traditional and new wastewater treatment systems use membrane separation techniques, which are the most cost-effective, highly selective, and easy to integrate with other processes. Membrane separation procedures are also the least harmful to the environment. Membrane separation techniques are also the least harmful to the environment of all the separation methods [6]. Ultrafiltration (UF) is a typical method for separating, purifying, and concentrating water-soluble solutes or dispersible-water compounds [7].

Polysulfone (PS) is a widely used material for ultrafiltration membranes (UF membranes) in a range of applications, including gas separation, wastewater treatment, and beverage and food processing. The polymer makes membrane manufacture easier because of its mechanical strength, chemical inertness, robust forming-film capabilities, configurable pore size, thermal stability, and repeatability. The inability of manufactured membranes to reject or adsorb tiny molecules, as well as the membrane's hydrophobic nature, causes this. To compensate for this limitation, organic/inorganic chemicals or nanomaterials can be injected into the membrane's dope solution as a third dimension. Polyvinylpyrrolidone (PVP), polyethylene glycol (PEG), propionic acid (PA), polyethylene oxide (PEO), surfactants, alcohols, and water are among the other regularly used additives [8–10]. The names of several UF membrane manufacturers are listed, with several of them producing multiple series of membranes (for example, regenerated cellulose, polysulfone, and cellulose acetate), each of which has a different molecular weight cut-off or pore size (for example, cellulose acetate membranes) [11]. Because of their high water solubility, organic solvent compatibility, low toxicity, complexing performance, and film-forming characteristics (PVP), UFM membranes produced by a conversion phase method are widely used as water-soluble polymers such as poly(ethylene glycol) (PEG) and poly(vinyl pyrrolidone) (PVP) [12]. Pores in these water-soluble polymers have a propensity to promote membrane surface pores and porosity, which is beneficial [10,13,14].

Membrane permeability, antifouling characteristics, and mechanical qualities have all lately improved, affecting the casting solution significantly. Nano-blending nanofibers such silica, silver, titanium nanoparticles, carbon nanotubes, and polyaniline (PANI) nanofibers have all been employed in UF membranes [15–21]. The number of tiny holes and membrane porosity rise as a large amount of nanomaterial is injected, but membrane pores lighten across the cross-sectional structure. Nanoparticles, unlike water-soluble polymers that promote membrane stability, can remain in the membrane formed indefinitely as an addition. The addition of a few nanoparticles may cause a considerable increase in membrane permeability [22]. Nanomaterials clump together because of their large specific surface area. The efficacy of nanoparticles in increasing membrane performance is reduced by agglomeration, which has a detrimental influence on the successful use of nanomaterials in nanocomposite membranes [19]. Mechanical dispersion (such as sonication and grinding) and chemical nanomaterial surface modification have both been explored to prevent nanomaterial aggregation. We employed sonication to break up the clumping of mesoporous silica nanosphere (MSN) in this work [19,23].

Mesoporous silicas, such as SBA-15 and MCM-41 silicas, are solid substances with a honeycomb-like porous structure and hundreds of empty channels. Because of their novel properties, such as tunable diameters of particles, convergent pore sizes with a narrow distribution, large pore volumes, and extensive surface areas. Mesoporous silica nanosphere (MSN) have recently been carefully explored in materials research [24] demonstrated the biocompatibility, high constructional stability, and chemical fluctuation of silica using semiconductor quantum dots coated with silica. In addition, mice have been used to test the biodegradability of silica particles. MSN with conditioned qualities can be employed for a variety of applications, including drug administration, enzyme adsorption, catalyst support, protein separation, cell labeling, and cell imaging [25].

Researchers are working nonstop to develop more comfortable techniques for producing MSN with regulated features, such as reduced particle sizes, adjustable pore diameters, large pore volumes, and high surface area. The most common ways for adjusting MSN characteristics are the use of additional reagents, for example pore expanders and/or surfactants with variable chain lengths. Changing the ratio of reagent concentrations in a typical reaction mixture would be cheaper and easier to get the same or better results [26].

In this study, we used mesoporous silica nanosphere (MSN) to increase the hydrophilic nature of PS ultrafiltration membranes, which increases selectivity and continuity in the membrane ultrafiltration process by creating new pores suitable for rejection of Crystal violet $C_{25}H_{30}ClN_3$ molecules, as well as the cohesiveness of the membrane matrix. To improve membrane performance, water-soluble polymers such as poly(vinyl pyrrolidone) (PVP) were used.

## 2. Material and methods

### 2.1. Materials

LCD MB Udel® P-3500 as polymer materials, SOLVAY Advanced Polymer Company's polysulfone (PS) was employed. Merck (Germany), supplied N,N-dimethylformamide (DMF) with an analytical purity of 99.5% as a solvent. Sigma-Aldrich provided the cetyltrimethylammonium bromide (CTAB) and tetraethyl orthosilicate (TEOS). LOBA Chemie supplied 40,000 poly(vinyl pyrrolidone) (PVP). Oxford Lab Fine Chem LLP provided the Crystal violet $C_{25}H_{30}ClN_3$.

### 2.2. Preparation of mesoporous silica nanospheres

At ambient temperature, mesoporous silica was created using CTAB as a template by hydrolysis of TEOS with an ammonia catalyst in a mixed solvent of acetone, water, and diethyl ether. CTAB (0.5 g) was usually added to bi-distilled water (100 mL) and stirred for 30 min before adding acetone (40 mL) and shaking for another 30 min before adding diethyl ether (20 g). After 30 min of vigorous

swirling, TEOS (2.5 mL) was added and swirled for another 30 min, then 1.5 mL of $NH_3OH$ was added and swirled for another 30 min (25 wt.%). The gel was rapidly stirred in a closed jar at 25°C for 24 h. The particles were captured via filtration, then washed with bi-distilled water and dried at 80°C for 24 h. Then calcination at 550°C for 4 h at room temperature, followed by another 8 h at 550°C [27].

### 2.3. Synthesis of PSF-UF membranes

All PS-UF membranes were prepared using the usual phase conversion method. In a nutshell, the neat PS ($M_0$) was dissolved in (15 wt.%) DMF and agitated vigorously for 6 h to achieve a homogeneous and transparent solution. PS/PVP membrane ($M_1$) was made by dissolving 2.4 wt.% PVP (Mw = 40,000) in DMF and stirring gently until a clear homogeneous solution was got. For preparing PS/PVP/$SiO_2$ membranes, different amounts of silica nanoparticles (2, 4, 6, and 8 wt.%) were dispersed in the casting solutions and coded as $M_2$, $M_3$, $M_4$, and $M_5$, respectively (Table 1), followed by ultrasonication for 30 min at (30 kHz) frequency to ensure a high dispersion of $SiO_2$ nanosphere. All polymer solutions were degassed for 24 h at room temperature before being cast onto a clean glass plate using a knife applicator with a perfect gap of 200 between the applicator knife and the glass plate. Defect-free membranes were got by immersing the plate in a clean water bath for a prolonged length of time before characterization and membrane performance testing [9].

### 2.4. Characterization of MSN

The X'PERT – PRO – PANalytical was used to get angle-small X-ray diffraction (SAXRD) patterns, while the Bruker D8 Discover Diffractometer with monochromated was used to obtain angle-wide X-ray diffraction (WAXRD) patterns. Using the Quantachrome Autosorb System, the adsorption/desorption isotherms were determined at 77 K. The samples were outgassed for 24 h at 80°F before being analyzed. The Brunauer–Emmett–Teller surface areas, volume-pore, and pore size distribution were all calculated using $N_2$ adsorption data. On the adsorption branch of the nitrogen isotherms, the Barrett–Joyner–Halenda (BJH) approach was used to derive pore size distributions. A Zeiss Leo SUPRA 55 microscope and field-emission scanning electron microscopy (FESEM) was used to take the images. There was no metal coating on the samples for FESEM analysis. A high-resolution transmission electron microscope (HR-TEM, Tecnai G20, FEI, and The Netherlands) was used for imaging, crystal structure reveal, and elemental analysis.

### 2.5. Membranes characterization

The materials were vacuum dried for 24 h at 40°C before characterization. To assess the membranes' water wettability, the water contact angle was measured using the sessile drop technique Kruss model DSA25B. A Hamiltonian syringe dripped drops of 8.0, 0.2, l volume on the membrane's surface, and photos were taken after a 5-s delay. The drop snake approach [28] was then used to compute the contact angles. Fourier-transform infrared spectroscopy (FT-IR) spectroscopy (Thermo Scientific Corp., Nicolet iS50, USA) was used in the 500 to 4,000 $cm^{-1}$ range. The surface and cross-sectional morphologies of the fabricated membranes were investigated using a scanning electron microscope (SEM, Quanta FEG 250) manufactured in the United States, with a 20 kV speeding up voltage and a spot size of 3.5 low vacuum modes. The CubiX[3] Diffractometer was used to get the membranes' X-ray diffraction (XRD) patterns.

Table 1
Casting solution composition for nanocomposite membrane preparation

| Membrane code number | PS (%) | MSN (%) | PVP (%) | DMF (%) |
|---|---|---|---|---|
| $M_0$ | 15 | 0 | 0 | 85 |
| $M_1$ | 15 | 0 | 2.4 | 82.6 |
| $M_2$ | 15 | 0.3 | 2.4 | 82.3 |
| $M_3$ | 15 | 0.6 | 2.4 | 82 |
| $M_4$ | 15 | 0.9 | 2.4 | 81.7 |
| $M_5$ | 15 | 1.2 | 2.4 | 81.4 |

### 2.6. Membranes performance evaluation

The UF penetration test was carried out using a basic permeation cell, as illustrated in Fig. 1. The HP4750 stirred cell is chemically resistant, high-pressure resistant, and capable of performing a wide range of membrane filtrations [34]. The permeability of the membranes to pure water was tested at pressures ranging from 1 to 5 bar. The volume flow was calculated as follows:

$$J_\upsilon = \frac{V}{At} \tag{1}$$

where $J$ is the permeate flow (L/$m^2$ h), $V$ is the volume of collected permeate solution (L), $A$ is the effective membrane area ($m^2$), and $t$ is the duration (h) [29]. A stirred cell filtration system connected to a nitrogen gas cylinder was used to test the membranes' dye rejection behavior (stirred cell, HP4750, cell diameter of 5.1 $cm^2$, processing capacity of 300 mL, effective filtration membrane area of 14.6 $cm^2$) (Fig. 1). 10 ppm Crystal violet $C_{25}H_{30}ClN_3$ was used in a dye permeation flux test. Filtration cycles were used to collect (50 mL) aliquots of dye solution, which were subsequently monitored using an Acculab UVS-90. Using a UV-Vis spectrophotometer, the rejection was calculated:

$$R = \left(1 - \frac{C_p}{C_f}\right) \times 100\% \tag{2}$$

where $R$ is the rejection (%), $C_p$ and $C_f$ are the concentration of permeate and feed solutions, respectively.

## 3. Results and discussions

### 3.1. MSN characterization

MSN were made in a basic solution with co-solvents ethyl ether, acetone, and water at room temperature using

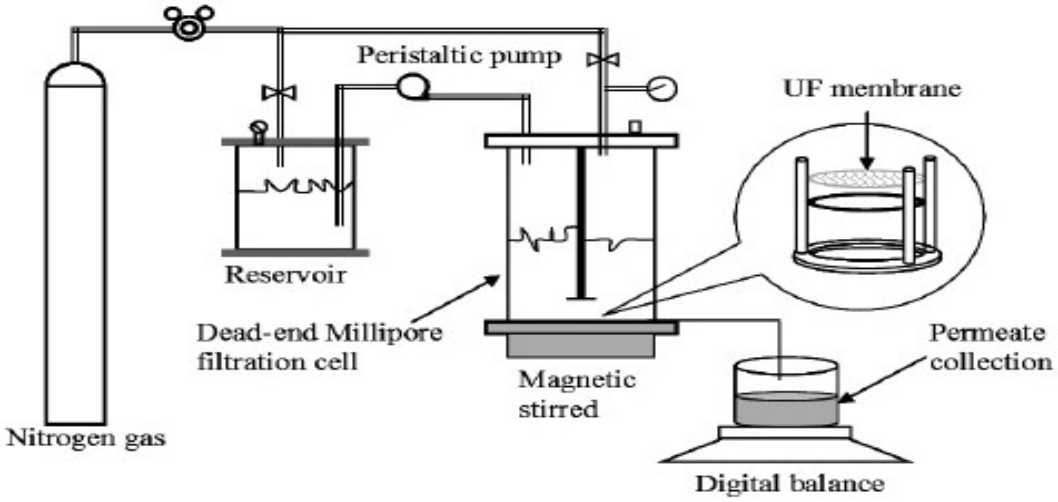


Fig. 1. UF permeation test unit schematic diagram.

a surfactant CTAB. The bonding of hydrogen between the molecules of water and ethyl ether, according to Chang et al. [30], provides a diffusion pathway for both surfactant and water to enter the TEOS/ethyl ether oil droplets, promoting the hydrolysis of TEOS, which then polymerizes with the surfactant and eventually turns into spheres via a soft silica gel. Acetone has proven to be a useful co-solvent for regulating nanoparticle shape and surface roughness, most likely because it is miscible with TEOS and water; hence, increasing the acetone percent in the mixed solvent reduces TEOS hydrolysis and homogenizes inorganic species polymerization [31]. Using acetone as a co-solvent appears to improve the mutual dissolution of water and ethyl ether, affecting the last structure and morphology. The ethyl ether nanodroplets would next be treated with acetone, water, ammonium hydroxide, and CTAB. Hydrolysis/condensation of TEOS and self-assembly of generated silica species occur simultaneously on the surface and in the interior of ethyl ether nanodroplets when TEOS is added to the aforementioned solution while aggressively whirling. Massive mesopores and even macropores form when ethyl ether is gasified, resulting in hierarchically porous silica nanospheres [32]. As illustrated in Fig. 6a, X-ray diffraction exhibits a significant diffraction peak between 17° to 30°, demonstrating typical infrequent changes in the electronic density because of the material's long-range ordering of the pores [26]. As shown in Fig. 2, the sample for FESEM evaluation had no metal coating (a). As illustrated in Fig. 2, a high-resolution transmission electron microscope was used for imaging (b). The FESEM image depicts 450 nm nanospheres, whereas the transmission electron microscopy image depicts massive slit-like mesopores uniformly spread over the nanosphere surface.

MSN's nitrogen adsorption/desorption isotherms are shown in Fig. 3a. The relative pressures of 0.3, 0.3–0.9, and 0.9 correspond to three distinct adsorption/desorption fractions. Small hysteresis loops can be seen in desorption regions with high relative pressure levels. Type IV isotherms were formed in the sorption studies, which are typical of mesoporous materials. Hysteresis loops were observed in

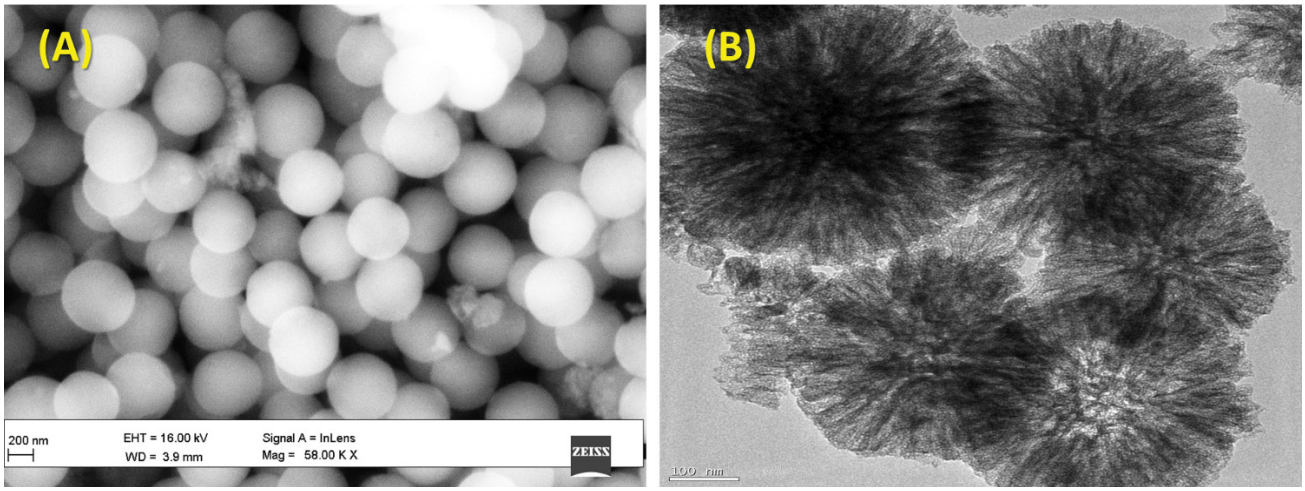


Fig. 2. (a) FESEM and (b) TEM images of the MSN.

mesopores and were connected to capillary condensation. The small pores with diameters of 3 nm in Fig. 3b match the typical mesoporous silica templated by CTAB and are thus assigned to the main channel of the composite, whereas MSN showed a significant distribution of mesopores with diameters of 25 nm, showing the dissolution of excess ethyl ether into the CTAB micelle to enlarge [33]. The Crystal violet molecule has a molecular cross-section of about 0.9 nm and can't go through holes smaller than 1.3 nm in diameter [34]. As a result, it can only pass through larger micropores (those larger than 1.3 nm), with most of it being absorbed in mesopores. As a result, MSN micropores are mostly larger pores. Therefore, a combination of pore size and surface chemical features may be responsible for MSN's higher adsorption. This shows that increasing the number of mesoporous silica nanospheres results in a significant reduction in Crystal violet rejection.

### 3.2. Membrane characterization

X-ray diffraction may determine the structure of PSF and nanocomposite PSF membranes (XRD). Fig. 4a shows the XRD spectrum of MSN, which shows a significant diffraction peak between 17° to 30°, revealing typical infrequent changes in the electronic density because of the long-range ordering of the pores in the material [26]. The XRD diffraction patterns of PS ($M_0$) are shown in Fig. 4b, with a large peak matching to the amorphous structure of PSF. Meanwhile, when MSN concentration grows, a sharp peak at 2 appears, which is because of the MSN

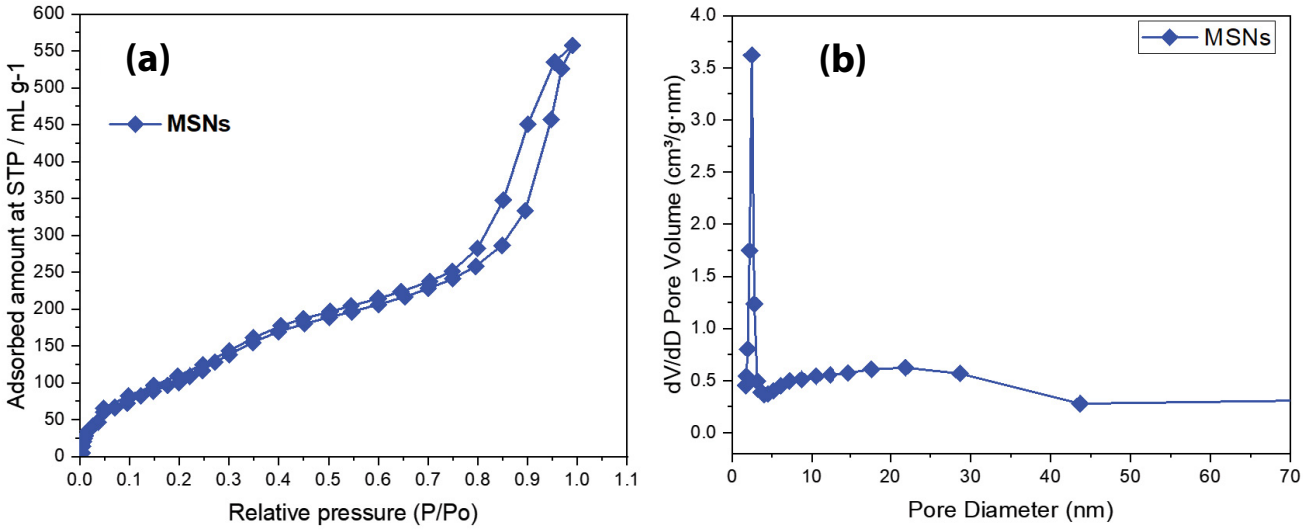


Fig. 3. Isotherms of nitrogen adsorption/desorption (a) and MSN pore size distribution (b).

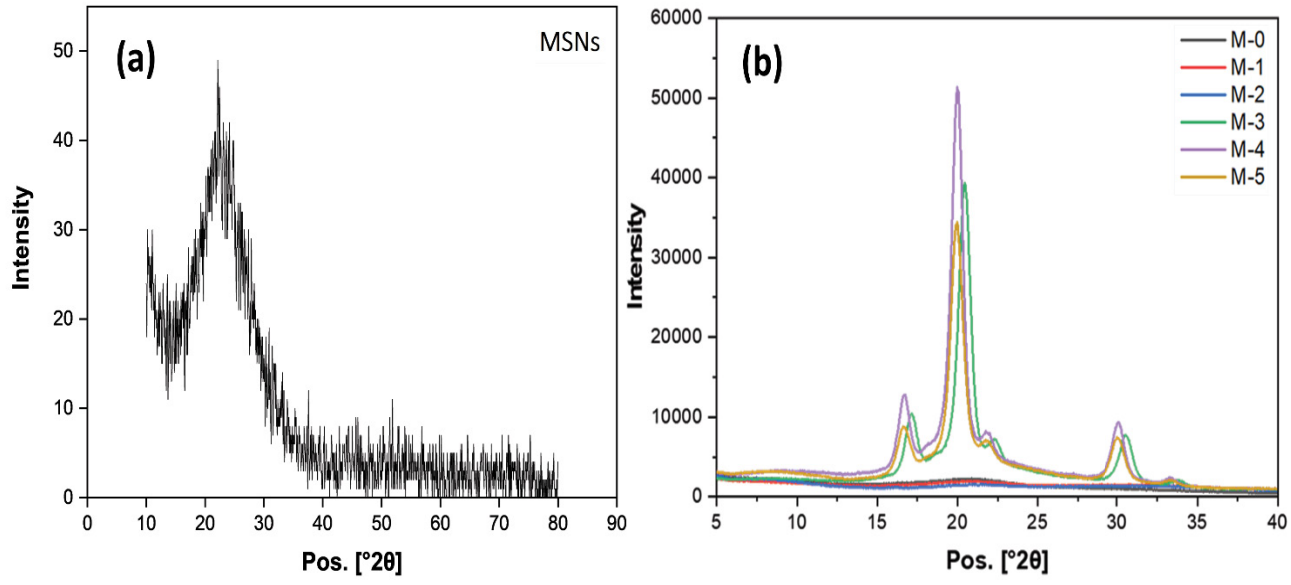


Fig. 4. MSN (a) and PS/MSN membranes with varied MSN contents X-ray diffraction pattern (b).

(violet color) – ($M_4$) membrane's high crystallinity. This revealed that, after mixing and employing the phase conversion approach, silica could still be discovered in PS/PVP membranes. It also reveals that MSN is dispersed throughout the membrane, although the amount used is relatively little.

The membranes› FT-IR spectra are shown in Fig. 5. Including silica, nanospheres resulted in remarkable peaks in the FT-IR spectra of membrane samples at 1,106 and 1,080 $cm^{-1}$. These peaks were ascribed to the asymmetric stretching vibration of Si–O–Si groups, implying the presence of $SiO_2$ particles inside the membranes [35]. The absorption peak at 800 $cm^{-1}$ is handled by the Si–O–Si symmetric stretching vibration. At 3,455 and 1,669 $cm^{-1}$, Si–OH stretching can manage the small sharp band. The membranes' FT-IR spectra are shown in Fig. 5. Including silica nanoparticles resulted in remarkable peaks in the FT-IR spectra of membrane samples at 1,106 and 1,080 $cm^{-1}$. These peaks were ascribed to the asymmetric stretching vibration of Si–O–Si groups, implying $SiO_2$ particles inside the membranes [36]. The absorption peak at 800 $cm^{-1}$ is handled by the Si–O–Si symmetric stretching vibration. At 3,455 and 1,669 $cm^{-1}$, Si–OH stretching can manage the small sharp band. Because of the presence of more hydrophilic functional groups in $SiO_2$ nanoparticles than in pure PS membranes, the PS/PVP/$SiO_2$ nanocomposite membranes are more hydrophilic than pure PS membranes. As a result of the presence of more hydrophilic functional groups in $SiO_2$ nanoparticles than in pure PS membranes, the PS/PVP/$SiO_2$ nanocomposite membranes are more hydrophilic than pure PS membranes. Two substantial absorptions at 1,487 and 1,585 $cm^{-1}$ point to C=C aromatic vibrational bonding in the polysulfone group, whereas the wavelength of 2,967 $cm^{-1}$ is associated with the bond (=C–H) vibration of the polysulfone aromatic ring [37,38].

Fig. 6 illustrates the surface properties of the membrane as measured by SEM imaging, demonstrating that the addition of a water-soluble polymer (PVP) smoothed the membrane surface and increased the hydrophilic nature of the pristine PSF membrane (Fig. 6b). Some researchers believe that the addition of additives is one of the most important factors influencing membrane shape and structure [10]. Chemicals are frequently used to develop optimal membrane designs, resulting in better membrane performance characteristics. They exhibited the effect of MSN content on surface form and membrane porosity in Figs. 6c–f, where MSN was found to be dispersed throughout the polymeric matrix's internal pores at all concentrations. XRD evidence (Fig. 4), which showed MSN in the polymer matrix, contradicts these findings. When compared to pristine PS membranes, SEM analysis of the top surface morphology revealed that the (MSN blended PS) membranes showed larger porosity. The porosity of PS/$SiO_2$ membranes was observed to grow because of two factors: (i) a rise in the number of pores, and (ii) an increase in the pore size [4]. According to SEM surface pictures, adding MSN to the casting solution increased the surface roughness of the PSF membrane, which is likely because nanoparticles break the homogeneity of polymeric chains on the surface [39]. Alongwith the epidermal layer, SEM scans revealed a thick layer of crystalline MSN particles with diameters ranging from 350 to 450 nm. $M_4$ membrane has a higher density of nanoscale surface pores than other membranes (Fig. 6e).

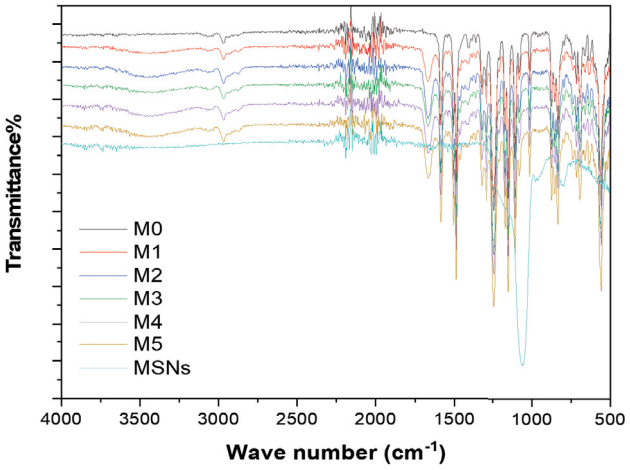


Fig. 5. MSN, unmodified membrane ($M_0$), and modified membranes FT-IR spectra.

The membranes' SEM cross-section images are displayed in Fig. 7. The spongy form of the plain PSF and PSF/PVP membranes can be seen, which may help with separation while reducing dye rejection [40]. A finger-like structure and a membrane substructure were transformed by introducing MSN. The nanoparticles were penetrated throughout the polymer matrix, resulting in finger-like structures and improved membrane pore interconnectivity. To demonstrate the impact of MSN on the internal structure of PSF membranes, the strategy used to prepare the porous PS membrane had to be shown, which included (a) adjusting the polymer content in the casting mixture, (b) adjusting the non-solvent bath temperature, and (c) increasing the content of mesoporous silica nanospheres. Because the solvent/non-solvent interchange happens faster in lower viscosity mixtures, permitting the fabrication of more porous materials [41], the casting mixture viscosity has a direct influence on the rate of gelation of the membranes. The influence of MSN fillers on the rheology of the casting solution was evaluated using visual information from the cross-sectional morphology, where the thick top layer was lowered from 61.24 to 33.54 m. The porous sublayer (macro voids) rose from 41.67 to 66.05 m, showing that microvoids were formed at low MSN concentration and subsequently repressed at higher MSN content (6 wt.%), which might be because of silica nanoparticles settling on the membrane surface, causing a thicker PVP layer to develop.

As the MSN concentration increased, water contact angle measurements decreased, showing that the membrane's hydrophilicity improved, potentially enhancing Crystal violet dye rejection. The $M_4$ membrane has been revealed to be exceptionally hydrophilic and acts as a dye barrier, enabling water molecules to pass through the pores of the membrane [3,42]. Because $SiO_2$ nanoparticles contain more hydrophilic functional groups than pure PS membranes, the PS/PVP/$SiO_2$ nanocomposite membranes are more hydrophilic than pure PS membranes, according to the contact angle values. Table 2 illustrates the effect of

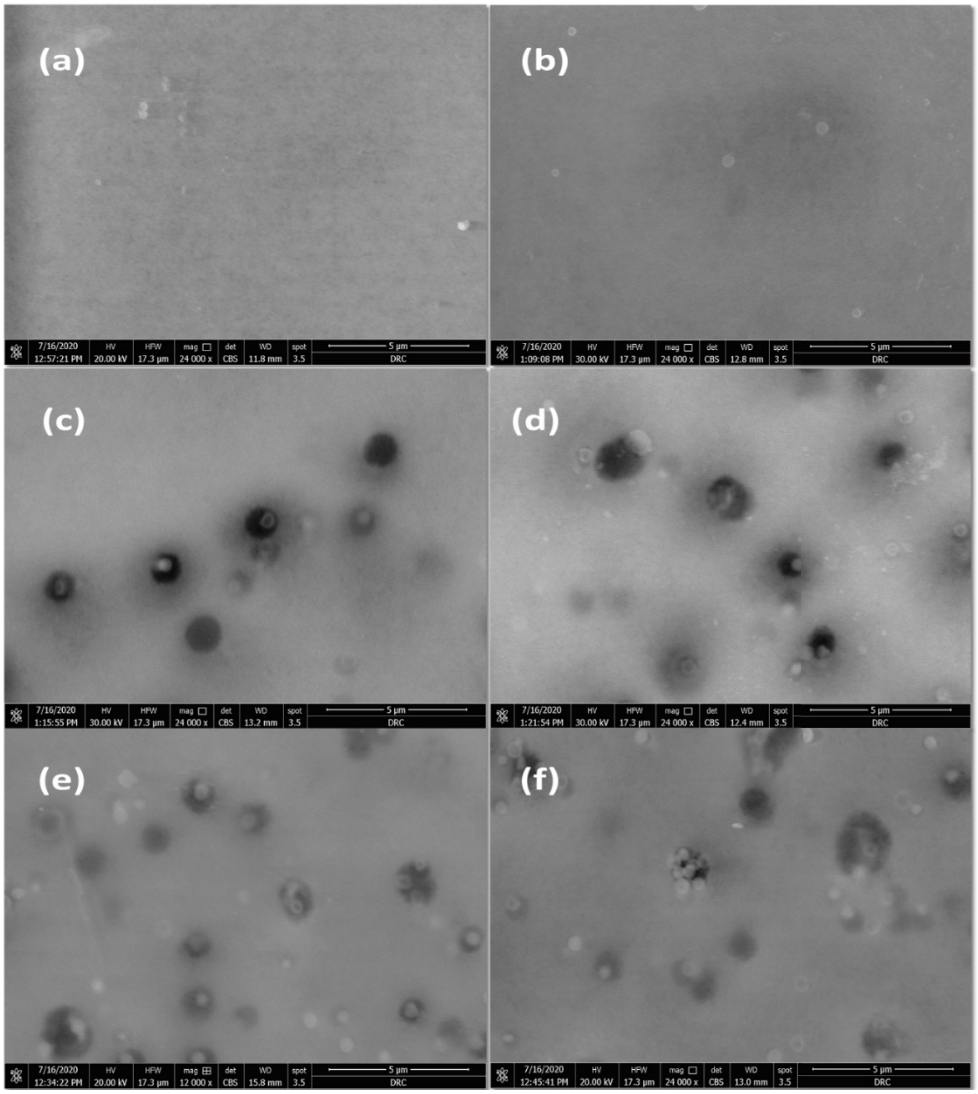


Fig. 6. SEM surface images of (a) PSF, (b) PSF/PVP, (c) PSF/PVP/MSN 2%, (d) PSF/PVP/MSN 4%, (e) PSF/PVP/MSN 6%, and (f) PSF/PVP/MSN 8%.

adding $SiO_2$ nanoparticles to PS/PVP/$SiO_2$ nanocomposite UF membranes on surface properties.

### 3.3. Membranes performance

Fig. 8 depicts the permeability of pure water through PSF ultrafiltration membranes at various pressures. The MSN concentration in the casting solution was gradually reduced as it climbed from $M_1$ to $M_4$. $M_1$'s was 415.9 L/m$^2$ h, whereas $M_4$'s was 122.7 L/m$^2$ h. Because PVP was added to the pure PSF casting solution, the resulting structure was thinner and more porous, resulting in increased hydraulic permeability. The addition of MSN to membranes alters their pore structure, either by deposition or by increasing membrane thickness. The membrane becomes denser as the thickness of the membrane support increases, and a sponge-like structure reduces the rate of water permeability through the membranes. When PVP was added to the polysulfone membrane, it transformed into a porous membrane with visible holes. It is well known that adding PVP to polysulfone membranes improves pore creation and permeation qualities; it is a potent pore-forming agent that gives the membranes ample time to work efficiently, but MSN acts as fillers, lowering membrane permeability.

Fig. 9 demonstrates how produced nanocomposite membranes, comprising varied quantities of $SiO_2$ nanoparticles and the pure polysulfone membrane, reject Crystal violet $C_{25}H_{30}ClN_3$. As a result, Crystal violet rejection for $M_0$ to $M_5$ membranes was 47.34%, 49.63%, 62.52%, 83.94%, 88.33%, and 55.52%, revealing that all PS/PVP/$SiO_2$ membranes outperformed pure PS membranes. Furthermore, when the number of $SiO_2$ nanoparticles in nanocomposite membranes rose, the rejection of Crystal violet increased. As a result, the highest rejection efficiency was attained, with about 88% separation efficiency, despite the $M_4$ membrane having a lower clean water flow than the others. To remove organic molecules (in this example, Crystal violet) via modified membranes, size exclusion (sieving, steric

effect), electrostatic discharges (electrical, Donnan), and adsorption on the membrane surface can all be utilized. Because of pore obstruction or narrowing produced by the precipitation of contaminating molecules, separation efficiency may be improved. The pollutant's physicochemical properties, solubility conditions, membrane characteristics, and operational circumstances are all factors that influence these processes [43]. Crystal violet molecules have a molecular cross-section of about 0.9 nm and can't go through holes smaller than 1.3 nm in diameter. As a result, it can only pass through larger micropores (those larger than 1.3 nm), with the majority of it being absorbed in mesopores. MSN nitrogen adsorption/desorption isotherms demonstrate that MSN micropores are mostly larger pores. As a result, the absorption mechanism influences separation efficiency significantly. Crystal violet molecules may be partially prevented from entering through membrane pores by the size exclusion process. Although dye rejection increased with increasing MSN concentration, the permeate flow decreased. For $M_0$ to $M_5$ membranes, water flow drops progressively from 169.8, 151, 132.9, 122.1, 97.9, and 100.1 L/m$^2$ h. Adding more $SiO_2$ nanoparticles (6 wt.%) to the casting solution viscosity lowers the amount of solvent (DMF)/non-solvent (water) exchange, resulting in a delayed phase separation action [44]. As a result, macro

Table 2
PS/PVP/$SiO_2$ membranes with varied silica content have various contact angles

| Membrane code number | Content of MSN (wt.% PSF) | Contact angle (°) |
|---|---|---|
| $M_0$ | 0 | 95.3 |
| $M_1$ | 0 | 92.3 |
| $M_2$ | 0.3 | 90.1 |
| $M_3$ | 0.6 | 89 |
| $M_4$ | 0.9 | 83.7 |
| $M_5$ | 1.2 | 82.3 |

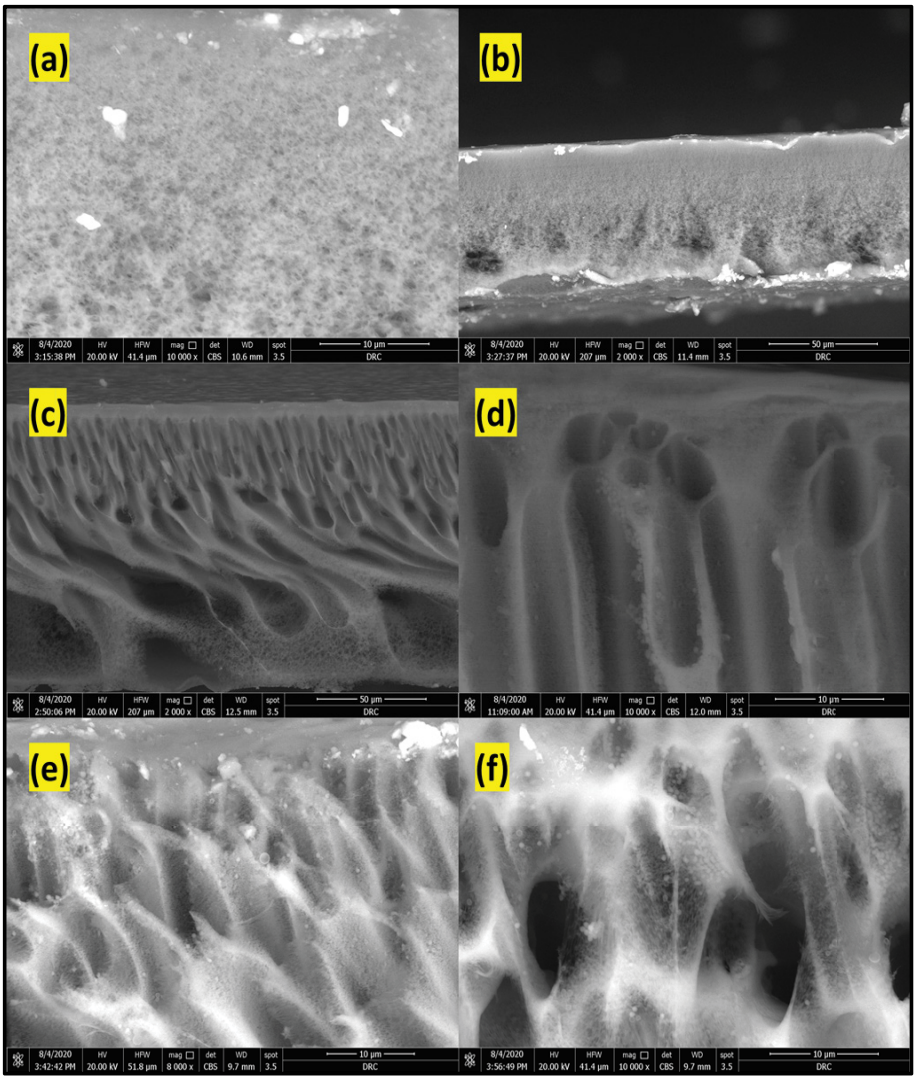


Fig. 7. Cross-sectional images of (a) PSF, (b) PSF/PVP, (c) PSF/PVP/MSN 2%, (d) PSF/PVP/MSN 4%, (e) PSF/PVP/MSN 6%, and (f) PSF/PVP/MSN 8%.

spaces in the membrane are prevented from forming or growing. As a result, the system's pores get smaller, the membrane sponge structure expands, and the membrane flow decreases ($M_4$). Fig. 7 depicts the fabricated membranes in cross-section. The pure PSF membrane, as seen, has a denser and more compact surface than membranes treated with $SiO_2$ nanoparticles, which may reduce water flow and therefore permeability.

## 4. Application

To assess the saturation of the membrane and test its efficacy, two samples of industrial wastewater were brought in: one from a ceramic industry in the industrial zone in the northwestern Gulf of Suez, and the other from a textile dyeing facility in the Delta area, where samples were prepared: The first sample, coded (50 mL), is an industrial drainage sample from ceramic factories where we noticed large quantities of mixed soil with the colors of tile and glaze used for polishing, so the sample was sedimented for 48 h, then a filter was made using several layers of cloth to separate the dust from the sample, and then the sample was sedimented again for another 48 h filter. The paper was used to separate the residual from extremely fine dust, and a bright blue color was seen with a blank absorption of 296 nm. Separation filtration and sample preparation were accomplished. Membranes $M_1$ and $M_4$ had 39.17% and 72.15% dye rejection, respectively, with a drop water flow from 176.84 to 123.66 L/m$^2$ h in a built cell at 1 bar pressure. The second sample, a textile factory industrial sample coded as (100 mL), was filtered with filter paper to remove impurities and tissue remnants, observe the purity of the purple color, and prepare the sample for separation by repeating the previous steps using the cell at 1 bar with a blank absorption of 300 nm. To appropriately treat textile wastewater, a membrane with strong dye rejection is required. The dye rejection percentages for membranes $M_1$ and $M_4$ were 53.12% and 93.2%, respectively, with a drop water flow from 156.17 to 100.61 L/m$^2$ h in the produced cell. The results of this study suggest that using nanocomposite membranes to remove pollutants like dyes from industrial wastewater resources is a viable option.

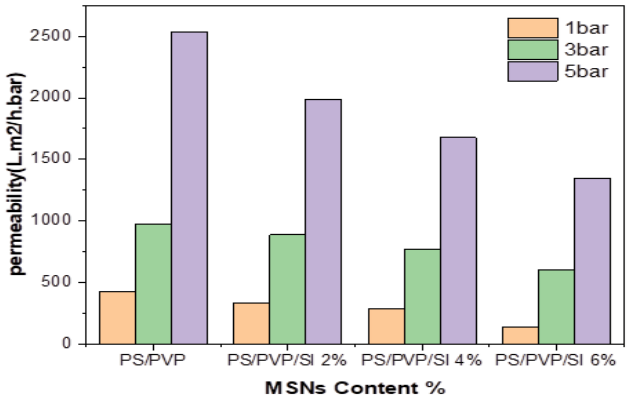


Fig. 8. Pure water permeability of the prepared membranes at different pressures as a function of MSN content.

## 5. Conclusions

PS membranes containing MSN nanoparticles were created using the phase conversion process, which comprised adding MSN directly to the casting solution. The presence of oxygen-containing groups in MSN significantly improved the membranes' hydrophilicity and permeability. Lowering the water contact angle confirmed the hydrophilicity of the PS/PVP/$SiO_2$ membranes. As illustrated in cross-sectional images, when MSN is added, the membrane's asymmetric structure changes from a sponge-shaped form with closed-end tear-like holes to a porous finger-like structure with open-end channels. Surface roughness increased as the MSN concentration in the polymer solution increased, according to SEM surface images. According to the findings of this study, the concentration of MSN nanoparticles is an important parameter

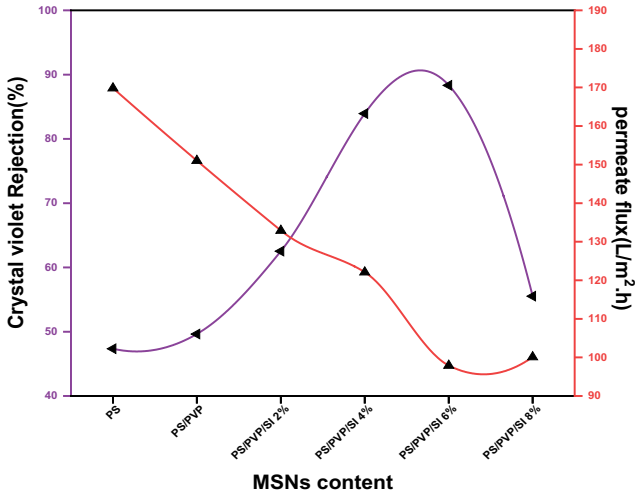


Fig. 9. Permeation flow of PS, PS/PVP/$SiO_2$ hybrid membranes and Crystal violet rejection as a function of MSN concentration (pressure = 1 bar, Crystal violet concentration = 10 ppm).

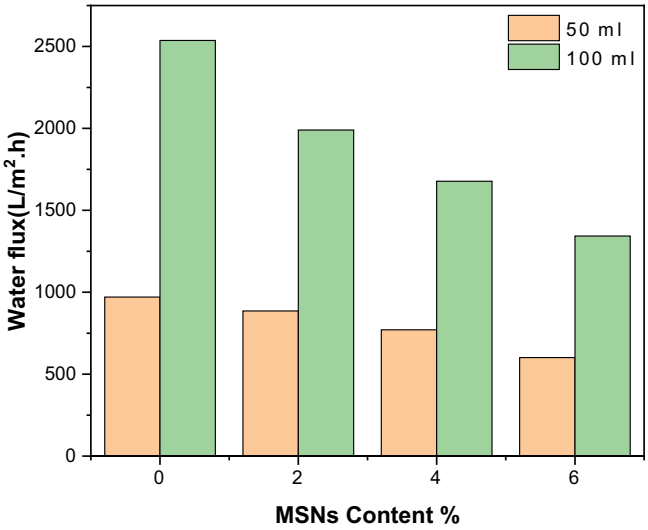


Fig. 10. Rejection and water flux of industrial wastewater sample through hybrid membranes as a function of MSN concentration.

that might affect the function and form of membranes. The optimal MSN concentration in the casting solution was discovered to be 6 wt.% due to dye permeate flux features and rejection qualities. The rejection of Crystal violet by the nanocomposite membranes developed was also significantly improved. The rate of Crystal violet retention increased as the concentration of MSN increased. The surface roughness increased as the MSN concentration in the polymer solution increased, according to SEM surface images. According to the findings of this study, the concentration of MSN nanoparticles is an important factor that can affect the function and form of membranes. The optimal MSN concentration in the casting solution was determined to be 6 wt.% due to dye permeate flux characteristics and rejection qualities. Crystal violet rejection by the nanocomposite membranes developed was also significantly improved. The rate of Crystal violet retention increased as MSN concentration increased.

## Acknowledgment

The authors address their appreciation to the Deputyship for Research and Innovation, Ministry of Education in Saudi Arabia, for funding this research work through the project number UQU-IF-P2-20-001.

## References

[1] A. Mollahosseini, A. Rahimpour, M. Jahamshahi, M. Peyravi, M. Khavarpour, The effect of silver nanoparticle size on performance and antibacteriality of polysulfone ultrafiltration membrane, Desalination, 306 (2012) 41–50.
[2] N. Koutahzadeh, M.R. Esfahani, P.E. Arce, Sequential use of UV/$H_2O_2$—(PSF/$TiO_2$/MWCNT) mixed matrix membranes for dye removal in water purification: membrane permeation, fouling, rejection, and decolorization, Environ. Eng. Sci., 33 (2016) 430–440.
[3] S. Mozia, M. Tomaszewska, A.W. Morawski, Photocatalytic membrane reactor (PMR) coupling photocatalysis and membrane distillation—effectiveness of removal of three azo dyes from water, Catal. Today, 129 (2007) 3–8.
[4] K. Rambabu, S. Velu, Modified cellulose acetate ultrafiltration composite membranes for enhanced dye removal, Int. J. Chem. Sci., 14 (2016) 195–205.
[5] C.J. Huang, B.M. Yang, K.-H. Chen, C.C. Chang, C. Kao, Application of membrane technology on semiconductor wastewater reclamation: a pilot-scale study, Desalination, 278 (2011) 203–210.
[6] W. Guo, H.H. Ngo, J. Li, A mini-review on membrane fouling, Bioresour. Technol., 122 (2012) 27–34.
[7] B. Chakrabarty, A.K. Ghoshal, M.K. Purkait, Ultrafiltration of stable oil-in-water emulsion by polysulfone membrane, J. Membr. Sci., 325 (2008) 427–437.
[8] M.E.A. Ali, A. Shahat, T.I. Ayoub, R.M. Kamel, Fabrication of high flux polysulfone/mesoporous silica nanocomposite ultrafiltration membranes for industrial wastewater treatment, Biointerface Res. Appl. Chem., 12 (2022) 7556–7572.
[9] S. Habibi, A. Nematollahzadeh, S.A. Mousavi, Nano-scale modification of polysulfone membrane matrix and the surface for the separation of chromium ions from water, Chem. Eng. J., 267 (2015) 306–316.
[10] B. Chakrabarty, A.K. Ghoshal, M.K. Purkait, Effect of molecular weight of PEG on membrane morphology and transport properties, J. Membr. Sci., 309 (2008) 209–221.
[11] S. El-Safty, A. Shahat, K. Ogawa, T. Hanaoka, Highly ordered, thermally/hydrothermally stable cubic Ia3d aluminosilica monoliths with low silica in frameworks, Microporous Mesoporous Mater., 138 (2011) 51–62.
[12] C. Zhao, J. Xue, F. Ran, S. Sun, Modification of polyethersulfone membranes – a review of methods, Prog. Mater. Sci., 58 (2013) 76–150.
[13] B. Chakrabarty, A.K. Ghoshal, M.K. Purkait, Preparation, characterization and performance studies of polysulfone membranes using PVP as an additive, J. Membr. Sci., 315 (2008) 36–47.
[14] M.J. Han, S.T. Nam, Thermodynamic and rheological variation in polysulfone solution by PVP and its effect in the preparation of phase inversion membrane, J. Membr. Sci., 202 (2002) 55–61.
[15] P. Aerts, I. Genne, S. Kuypers, R. Leysen, I. Vankelecom, P. Jacobs, Polysulfone–aerosil composite membranes: Part 2. The influence of the addition of aerosil on the skin characteristics and membrane properties, J. Membr. Sci., 178 (2000) 1–11.
[16] P. Aerts, I. Genne, S. Kuypers, R. Leysen, I. Vankelecom, P. Jacobs, Polysulfone–aerosil composite membranes: Part 1. The influence of the addition of aerosil on the formation process and membrane morphology, J. Membr. Sci., 176 (2000) 63–73.
[17] Z. Fan, Z. Wang, N. Sun, J. Wang, S. Wang, Performance improvement of polysulfone ultrafiltration membrane by blending with polyaniline nanofibers, J. Membr. Sci., 320 (2008) 363–371.
[18] S. Qiu, L. Wu, X. Pan, L. Zhang, H. Chen, C. Gao, Preparation and properties of functionalized carbon nanotube/PSF blend ultrafiltration membranes, J. Membr. Sci., 342 (2009) 165–172.
[19] A. Razmjou, J. Mansouri, V. Chen, The effects of mechanical and chemical modification of $TiO_2$ nanoparticles on the surface chemistry, structure and fouling performance of PES ultrafiltration membranes, J. Membr. Sci., 378 (2011) 73–84.
[20] J.S. Taurozzi, H. Arul, V.Z. Bosak, A.F. Burban, T.C. Voice, M.L. Bruening, V.V. Tarabara, Effect of filler incorporation route on the properties of polysulfone–silver nanocomposite membranes of different porosities, J. Membr. Sci., 325 (2008) 58–68.
[21] Y. Yang, H. Zhang, P. Wang, Q. Zheng, J. Li, The influence of nano-sized $TiO_2$ fillers on the morphologies and properties of PSF-UF membrane, J. Membr. Sci., 288 (2007) 231–238.
[22] A. Sotto, A. Boromand, R. Zhang, P. Luis, J.M. Arsuaga, J. Kim, B. Van der Bruggen, Effect of nanoparticle aggregation at low concentrations of $TiO_2$ on the hydrophilicity, morphology, and fouling resistance of PES–$TiO_2$ membranes, J. Colloid Interface Sci., 363 (2011) 540–550.
[23] M. Sun, Y. Su, C. Mu, Z. Jiang, Improved antifouling property of PES ultrafiltration membranes using additive of silica–PVP nanocomposite, Ind. Eng. Chem. Res., 49 (2010) 790–796.
[24] S.A. El-Safty, A. Shahat, M.M. Mahmoud, H. Nguyen, W. Warkocki, M. Ohnuma, Mesoporous silica nanotubes hybrid membranes for functional nanofiltration, Nanotechnology, 21 (2010) 375603.
[25] V. Cauda, A. Schlossbauer, J. Kecht, A. Zürner, T. Bein, Multiple core–shell functionalized colloidal mesoporous silica nanoparticles, J. Am. Chem. Soc., 131 (2009) 11361–11370.
[26] A. Shahat, H.M.A. Hassan, M.F. El-Shahat, O. El Shahawy, M.R. Awual, A ligand-anchored optical composite material for efficient vanadium(II) adsorption and detection in wastewater, New J. Chem., 43 (2019) 10324–10335.
[27] A. Shahat, S. Trupp, Sensitive, selective, and rapid method for optical recognition of ultra-traces level of Hg(II), Ag(I), Au(III), and Pd(II) in electronic wastes, Sens. Actuators, B, 245 (2017) 789–802.
[28] A.F. Stalder, G. Kulik, D. Sage, L. Barbieri, P. Hoffmann, A snake-based approach to accurate determination of both contact points and contact angles, Colloids Surf., A, 286 (2006) 92–103.
[29] H. Matsuyama, T. Maki, M. Teramoto, K. Kobayashi, Effect of PVP additive on porous polysulfone membrane formation by immersion precipitation method, Sep. Sci. Technol., 38 (2003) 3449–3458.
[30] C.L. Chang, H.S.J.L. Fogler, Controlled formation of silica particles from tetraethyl orthosilicate in nonionic water-in-oil microemulsions, Langmuir, 13 (1997) 3295–3307.

[31] W.N. El-Sayed, K.Z. Elwakeel, A. Shahat, M.R. Awual, Investigation of novel nanomaterial for the removal of toxic substances from contaminated water, RSC Adv., 9 (2019) 14167–14175.
[32] X. Du, J.J.L. He, Fine-tuning of silica nanosphere structure by simple regulation of the volume ratio of co-solvents, Langmuir, 26 (2010) 10057–10062.
[33] F.N. Gu, W.G. Lin, J.Y. Yang, F. Wei, Y. Wang, J.H. Zhu, Fabrication of centimeter-sized sphere of mesoporous silica with well-defined hollow nanosphere topology and its high performance in adsorbing phenylalanine, Microporous Mesoporous Mater., 151 (2012) 142–148.
[34] A. Wathukarage, I. Herath, M.C.M. Iqbal, M. Vithanage, Mechanistic understanding of Crystal violet dye sorption by woody biochar: implications for wastewater treatment, Environ. Geochem. Health, 41 (2019) 1–15.
[35] S.A. El-Safty, A. Shahat, M. Ismael, Mesoporous aluminosilica monoliths for the adsorptive removal of small organic pollutants, J. Hazard. Mater., 201–202 (2012) 23–32.
[36] G.M. El Shafei, M.M. Mokhtar, Interaction between molybdena and silica: FT-IR/PA studies of surface hydroxyl groups and pore structure assessment, Colloids Surf., A, 94 (1995) 267–277.
[37] M. Shakak, R. Rezaee, A. Maleki, A. Jafari, M. Safari, B. Shahmoradi, H. Daraei, S.M. Lee, Synthesis and characterization of nanocomposite ultrafiltration membrane (PSF/PVP/$SiO_2$) and performance evaluation for the removal of amoxicillin from aqueous solutions, Environ. Technol. Innovation, 17 (2020) 100529, doi: 10.1016/j.eti.2019.100529.
[38] D. Nasirian, I. Salahshoori, M. Sadeghi, N. Rashidi, M. Hassanzadeganroudsari, Investigation of the gas permeability properties from polysulfone/polyethylene glycol composite membrane, Polym. Bull., 77 (2020) 5529–5552.
[39] M.R. de Moura, L.H.C. Mattoso, V. Zucolotto, Development of cellulose-based bactericidal nanocomposites containing silver nanoparticles and their use as active food packaging, J. Food Eng., 109 (2012) 520–524.
[40] A.R. Hassan, S. Rozali, N.H.M. Safari, B.H. Besar, The roles of polyethersulfone and polyethylene glycol additive on nanofiltration of dyes and membrane morphologies, Environ. Eng. Res., 23 (2018) 316–322.
[41] K. Boussu, C. Vandecasteele, B.J.P. Van der Bruggen, Study of the characteristics and the performance of self-made nanoporous polyethersulfone membranes, Polymer, 47 (2006) 3464–3476.
[42] M. Gryta, M. Tomaszewska, J. Grzechulska, A. Morawski, Membrane distillation of NaCl solution containing natural organic matter, J. Membr. Sci., 181 (2001) 279–287.
[43] S.O. Ganiyu, E.D. van Hullebusch, M. Cretin, G. Esposito, M.A. Oturan, Coupling of membrane filtration and advanced oxidation processes for removal of pharmaceutical residues: a critical review, Sep. Purif. Technol., 156 (2015) 891–914.
[44] E. Saljoughi, S.M.J.S. Mousavi, Preparation and characterization of novel polysulfone nanofiltration membranes for removal of cadmium from contaminated water, Sep. Purif. Technol., 90 (2012) 22–30.